3.e. Active Polymer Gels

Lit.: – T. Sawey et al., Science, 292, 2001
– D. Humphrey et al., Nature, 416, 2002

(i) self organization of microtubles and motors

molecular motors overcome entropy ⇒
disorder → order

non-equilibrium self organization
shear transparency

(ii) molecular motors overcome Brownian polymer dynamics

slow transparency

motors induce filament sliding
and overcome inherently slow and
random Brownian driven polymer motion

⇒ shear relaxtion times decrease!

+ crosslinkers ⇒ strain hardening!

3. Cell Motility

Lit.: - T. C. Pollard, G. G. Borisy, Cell, 2003
- Molecular Cell Biology, Lodish et al Chapt 18+19
- S. Wiesner et al, JCB, 160, 2003

show movies of motile cells!

show transparency cell motility 0

show transparency cell motility 1

(i) actin polymeration driven bead motility

show transparency bead motility 1+2

(ii) thermal ratchets

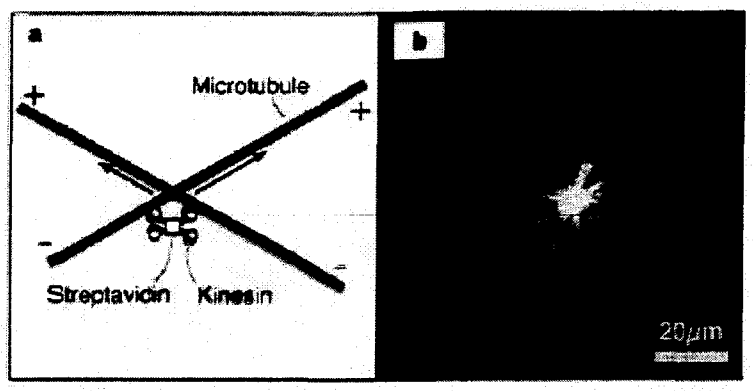

Figure 1 Self-organization of taxol-stabilized microtubules and kinesin constructs into asters. **a**, Schematic representation of a kinesin–streptavidin construct moving simultaneously along two microtubules. The kinesin constructs can be seen as force-generating, mobile crosslinks. **b**, A self-organized aster observed by dark-field microscopy. Polymerized and taxol-stabilized microtubules were mixed with motor constructs and ATP. The sample is shown after ~2 min. The bright spot in the centre of the aster is caused by light scattering from accumulated microtubules and motors. In cells and cell-free extracts, where the asters are organized by minus-end directed motors such as dyneins[5–7], the aster polarity is opposite. Scale bar, 20 μm.

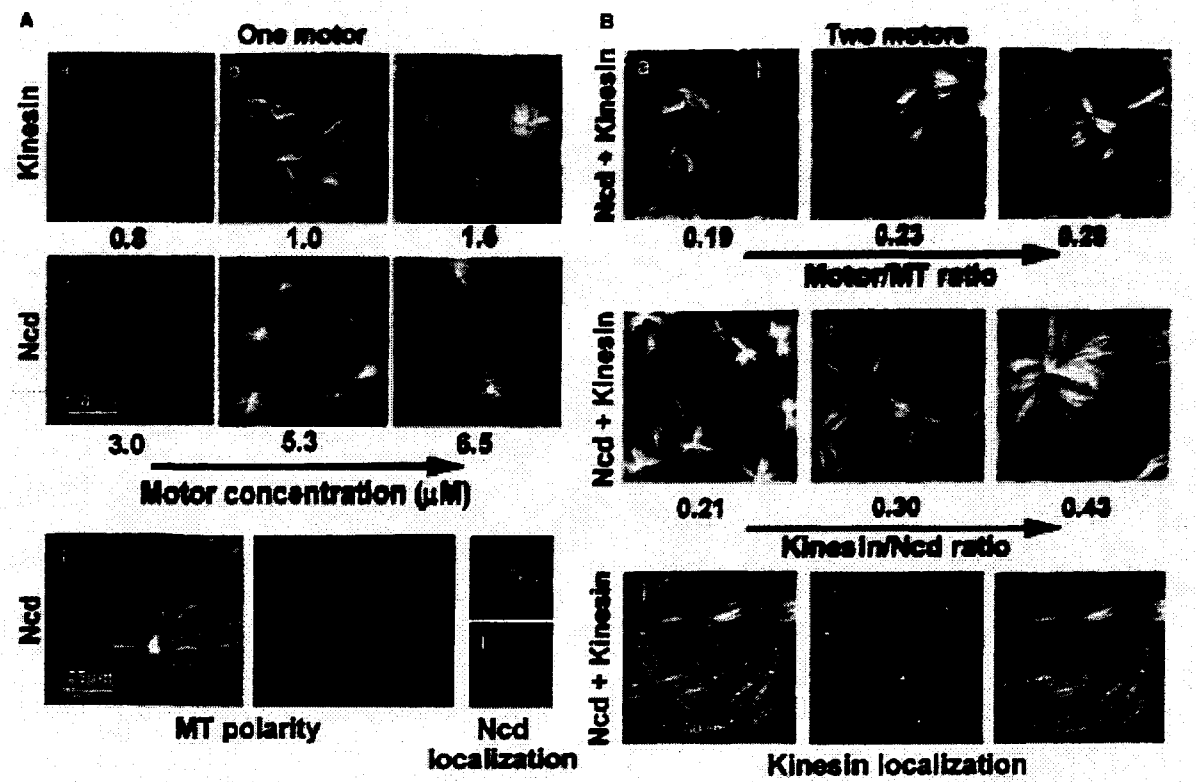

Fig. 2. MT patterns organized in vitro by the action of multimeric motor complexes. (A) One species of motor complex: Variation of the concentration of multimeric kinesin complexes (a to c) and of multimeric Ncd complexes (d to f). MTs are visualized by dark-field microscopy. The concentrations of the monomeric motors are indicated. The kinesin (monomer)/streptavidin (tetramer) ratio was maintained at 16, and the GST-Ncd (monomer)/anti-GST ratio at 5.3. Tubulin concentrations were 26 μM in kinesin experiments (a to c) and 23 μM in Ncd experiments (d to f). MT orientation in Ncd asters is shown with tetramethylrhodamine-labeled polarity-marked MT seeds (g: darkfield, h: fluorescence). The bright part of the seeds indicates the minus end. Motor localization is shown in asters organized by tetramethylrhodamine-labeled Ncd complexes (i: dark-field, j: fluorescence). (B) Simultaneous action of multimeric kinesin and multimeric Ncd: Variation of the motor/tubulin ratio (without changing the Ncd/kinesin ratio) (a to c). The concentrations of kinesin, Ncd, and tubulin were 1.2, 4.0, and 28 μM (a); 1.5, 4.9, and 28 μM (b); and 1.7, 5.6, and 26 μM (c), respectively. Variation of the kinesin/Ncd concentration ratio (d to f). Kinesin and Ncd concentrations were 1.2 and 5.6 μM (d), 1.7 and 5.6 μM (e), and 2.0 and 4.6 μM (f), respectively. The tubulin concentration was 28 μM. The localization of kinesin in MT networks is shown with the use of fluorescein-labeled kinesin (g: dark-field, h: fluorescence, i: overlay; conditions as in c). Images were taken 10 to 20 min (A) or 25 to 30 min (B) after the start of MT polymerization. For methods, see (12, 28).

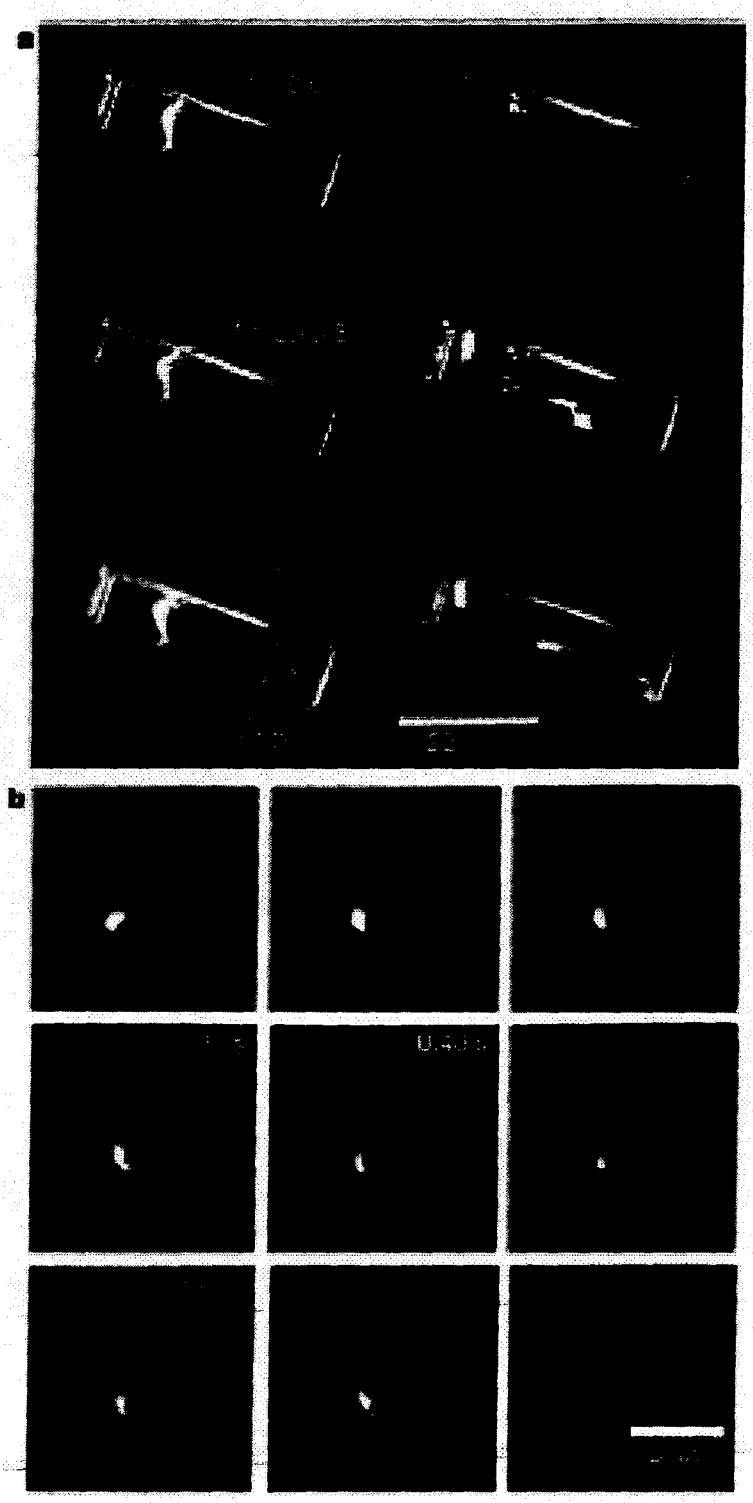

Figure 1 Macroscopic and microscopic influence of bipolar myosin minifilaments on actin networks. **a**, Comparison of the flow properties of actin networks with inactive (left side) or active (right side) myosin dispersed in them. For this purpose a cuvette filled to one-third with sample was lifted from its initial vertical position. With ADP and inactive myosin the samples gelated and behaved like an elastic solid. In the presence of ATP or when caged ATP was released, the active motors caused fluid-like flow properties. **b**, In the presence of ATP, two rhodamine–phalloidin-labelled actin filaments in dilute solution slide along each other while connected by BODIPY FL-labelled myosin (bright spot). The left filament moves to the upper left side with respect to the myosin minifilament and the right filament moves to the right. In the last picture filaments disengage.

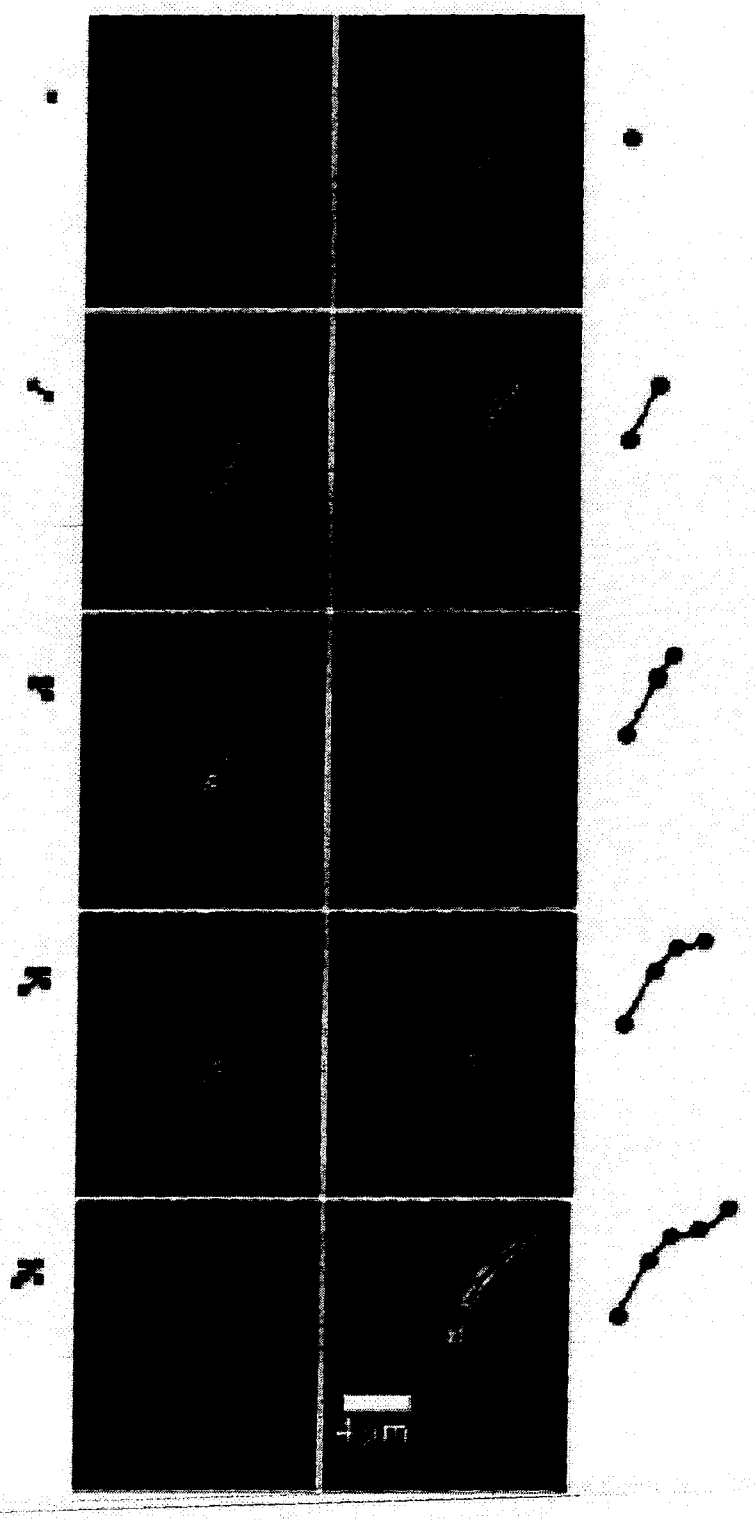

Figure 3 Motion of a single actin filament in an F-actin solution or an actin–myosin network. Fluorescently labelled filaments are embedded in an unlabelled matrix of filaments (left side) or in an unlabelled network of filaments with active myosin minifilaments present (right side). The time interval between successive pictures is 2.5 s. The left filament solely undergoes brownian motion restricted by the surrounding filaments. Within 10 s no net transport of the polymer chain was observed. The right filament shows directional sliding induced by myosin, resulting in a quick transport of the filament. The dashed black lines represent the digital traces of filament contours used to analyse filament motion. The two outer columns depict the motion of the upper filament ends without (squares) and with (circles) myosin.

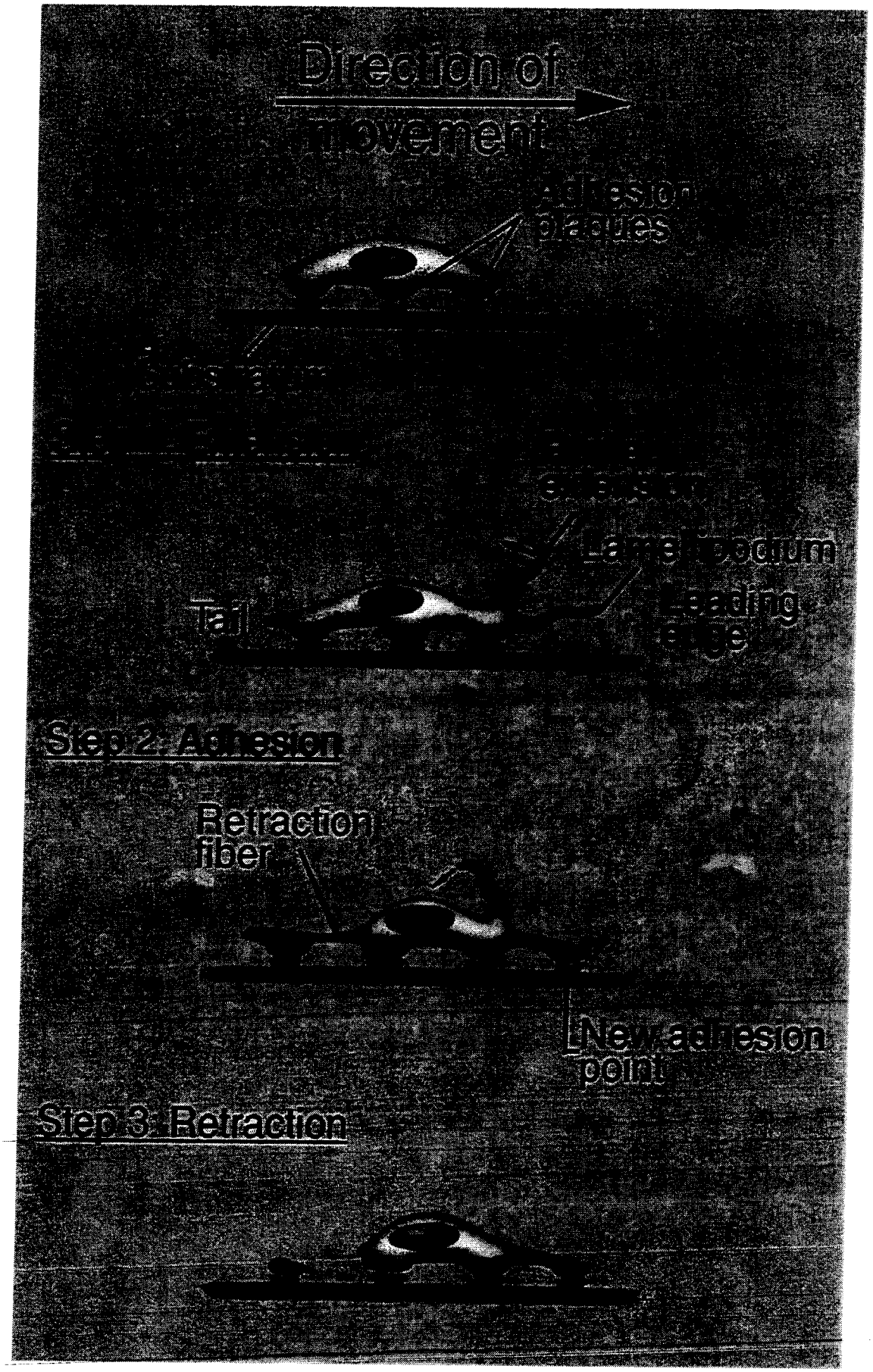
Direction of movement
Adhesion plaques
Tail
Step 2: Adhesion
Retraction fiber
New adhesion point
Step 3: Retraction

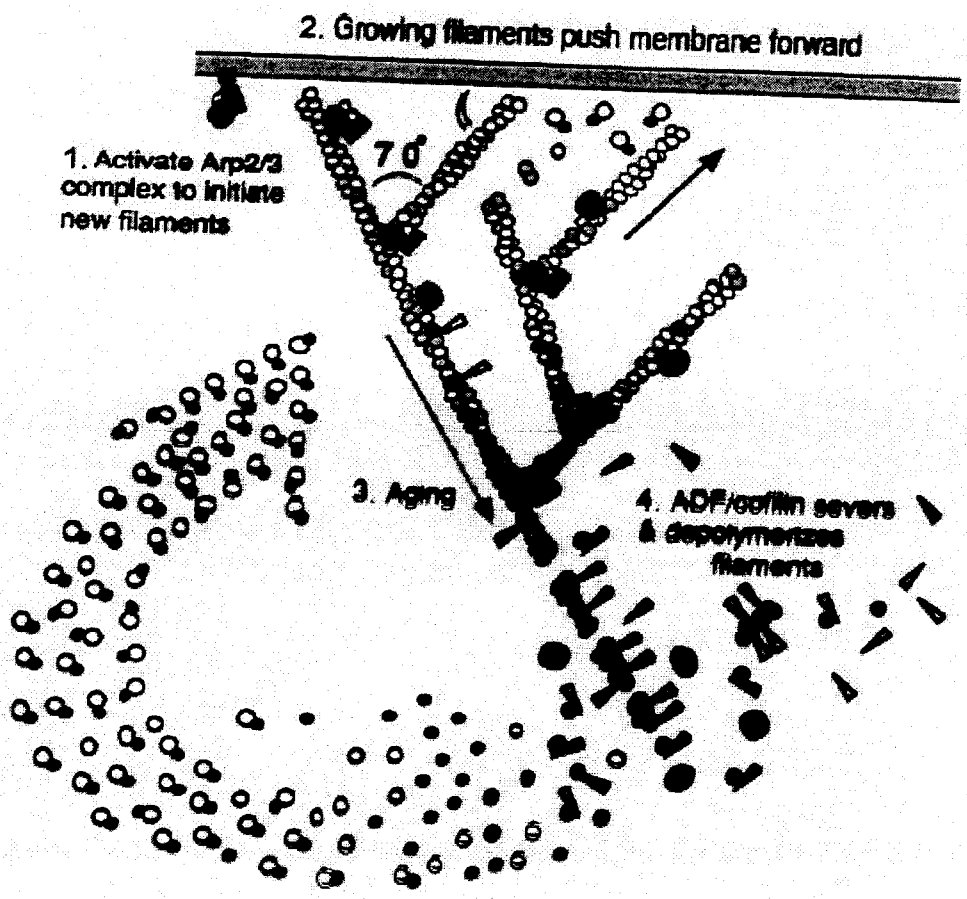
2. Growing filaments push membrane forward
1. Activate Arp2/3 complex to initiate new filaments
70°
3. Aging
4. ADF/cofilin severs & depolymerizes filaments

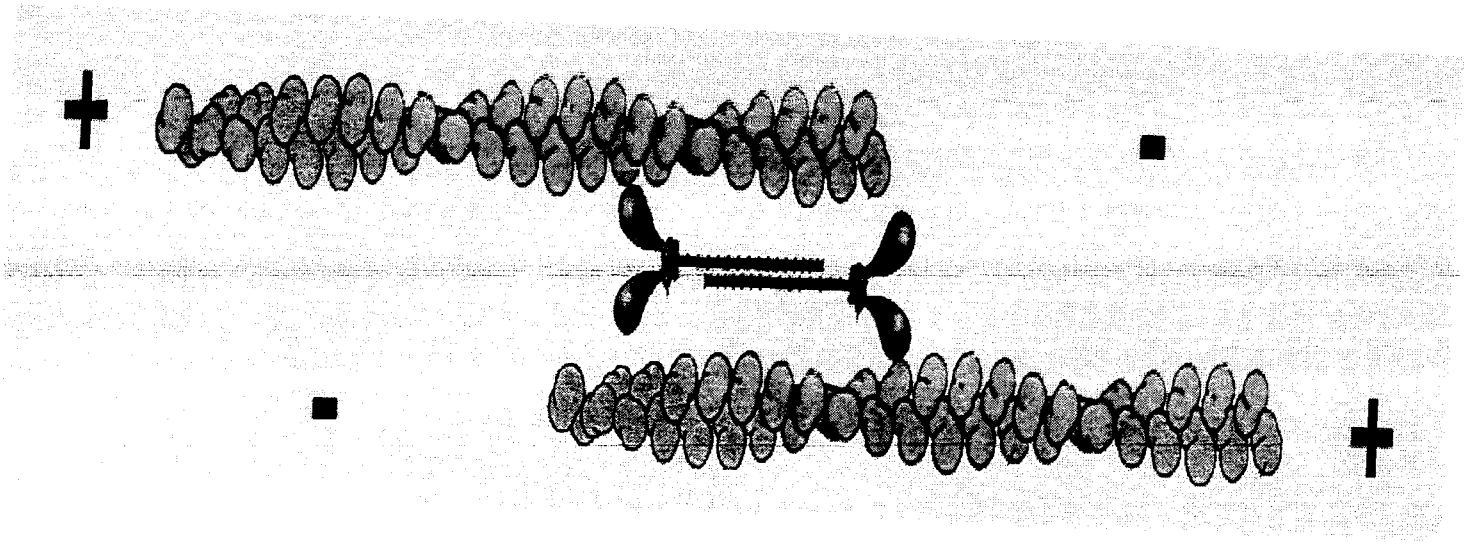

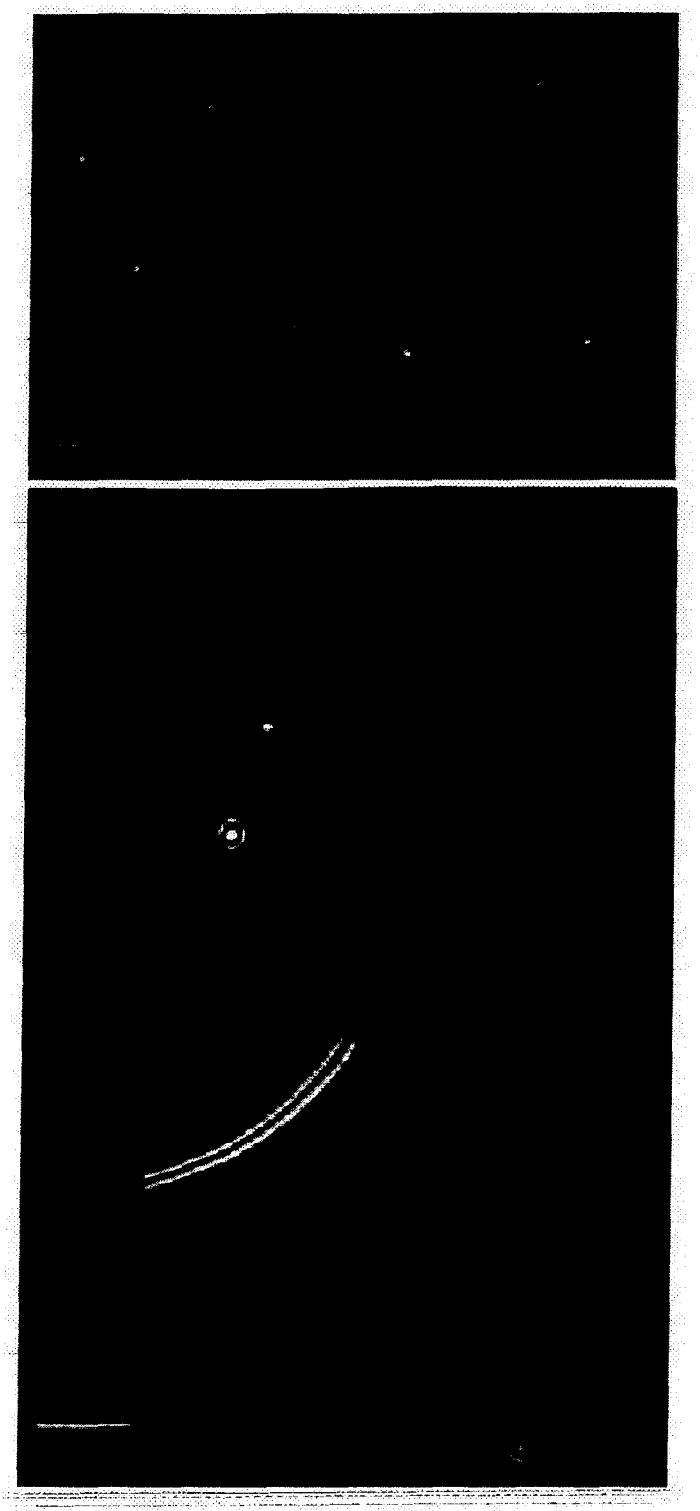

Figure 4. Biomimetic motility assay: Examples of actin-based motility of functionalized particles in the reconstituted motility medium. **Top:** N-WASP-coated beads (2 μm in diameter) generate actin tails and undergo propulsion in the medium. **Middle:** Beads of three different diameters (3, 1, and 0.5 μm) move at the same rate in the medium but display actin tails of different thickness. **Bottom:** A glass rod (1 μm diameter, 30 μm in length) generates a lamellar actin array and moves mimicking lamellipodium extension.

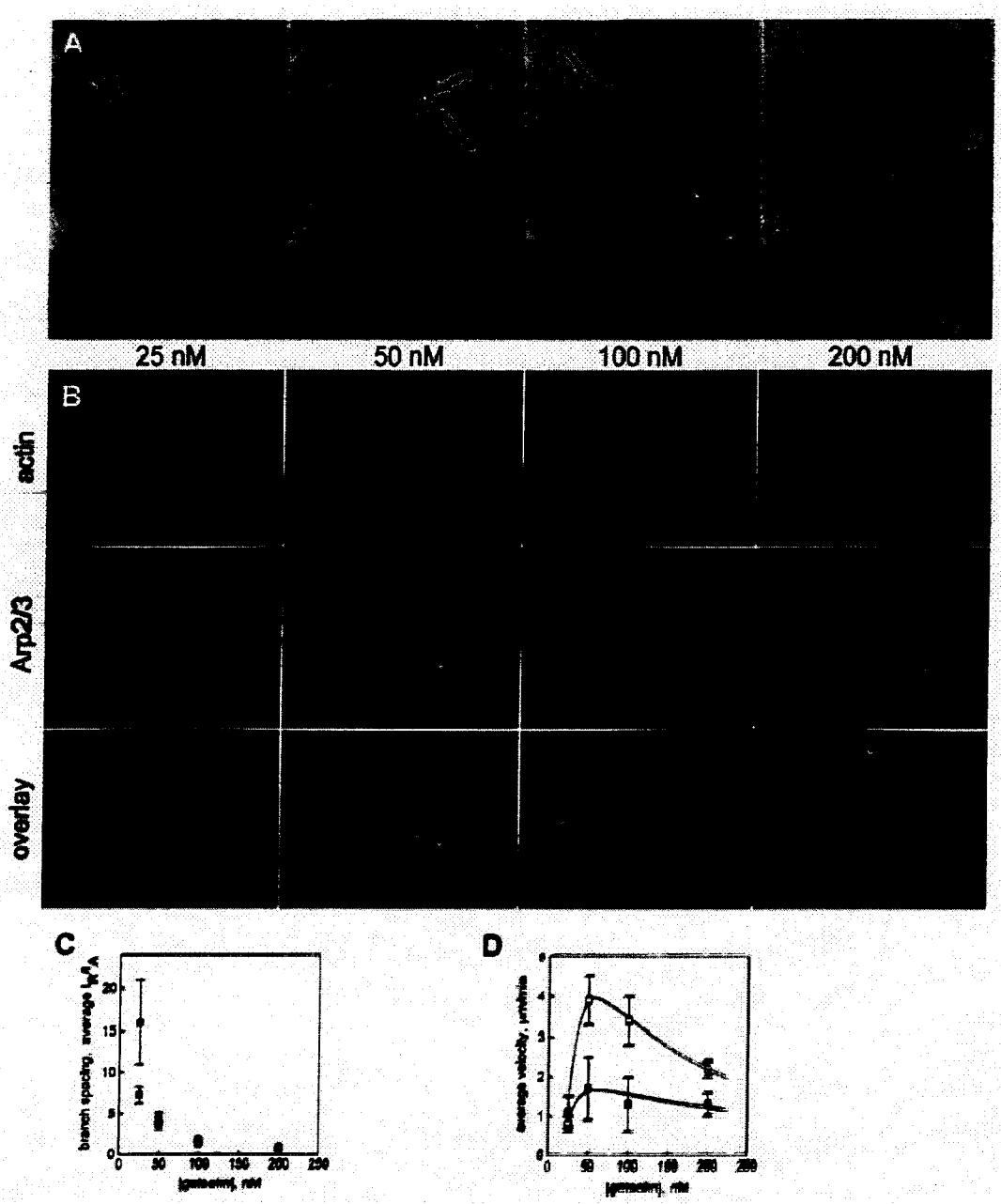

Figure 7. **Evaluation of the branch spacing in actin tails dependence on gelsolin.** (A) Typical images of tail morphologies for high-density beads (diameter 2 μm) at the indicated gelsolin concentrations. Note the presence of "fishbone" actin tails at low gelsolin, as previously reported (Pantaloni et al., 2000), and the decrease in tail length upon increasing gelsolin. (B) Quantitation of actin (rhodamine labeled) and Arp2/3 (Alexa®488 labeled) in the actin tails at different concentrations of gelsolin. The gallery shows typical images of high-density beads (diameter 2 μm) at indicated gelsolin concentrations. Alexa® fluorescence is saturated on the beads at 100 and 200 nM gelsolin. Note the decrease in the intensities ratio (I_B/I_A) as the gelsolin concentration increases. (C) Branch spacing is a decreasing function of the filament capping rate. Average I_B/I_A ratios were determined for sets of high-density (d_c = 0.064, pink squares) and low-density beads (d_c = 0.016, blue squares) at different gelsolin concentrations. For both bead types, branch spacing decreases sharply upon increasing the gelsolin concentration. (D) Bead velocity shows a bell-shaped dependence on filament capping. Average velocities are shown for high-density (d_c = 0.064, open squares/pink curve) and low-density beads (d_c = 0.016, closed squares/blue curve) at varying gelsolin concentrations.

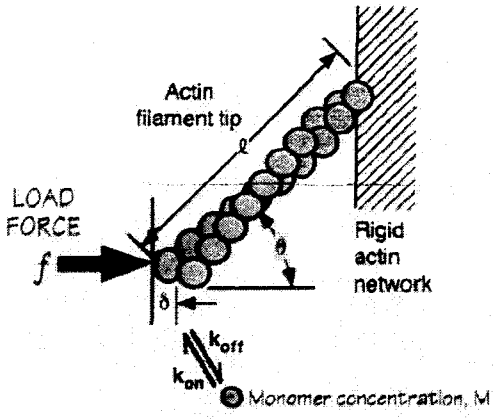
Actin
filament tip
LOAD
FORCE
f
Rigid
actin
network
δ
k_{off}
k_{on}
Monomer concentration, M

(a)

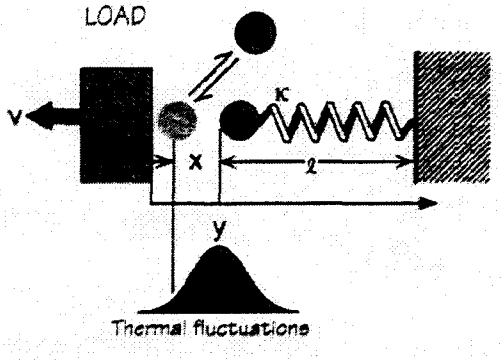
LOAD
V
κ
X
y
Thermal fluctuations

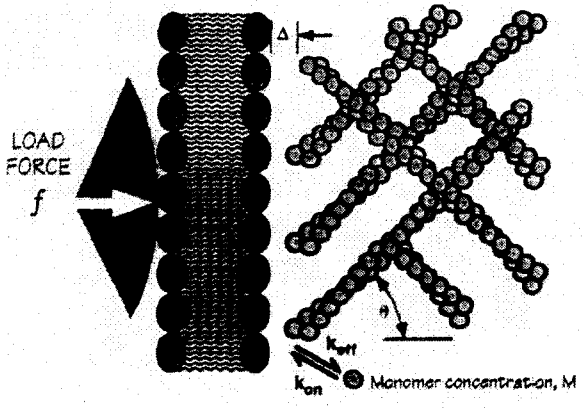
Δ
LOAD
FORCE
f
k_{off}
k_{on}
Monomer concentration, M

(a)

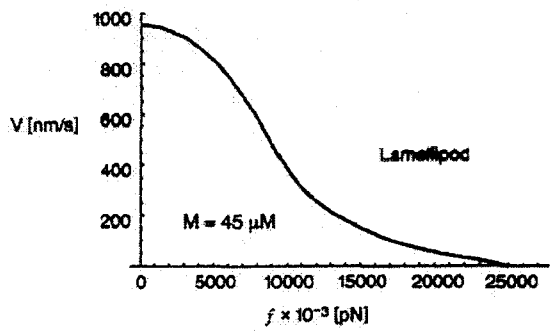
1000
800
V [nm/s]
600
400
200
Lamellipod
M = 45 μM
0
5000
10000
15000
20000
25000
$f \times 10^{-3}$ [pN]